Surgical Innovation
20(1) 59–69
© The Author(s) 2013
Reprints and permission:
sagepub.com/journalsPermissions.nav
DOI: 10.1177/1553350612438416
http://sri.sagepub.com
SAGE

Multimodal Imaging and Detection Strategy With 124 I-Labeled Chimeric Monoclonal Antibody cG250 for Accurate Localization and Confirmation of Extent of Disease During Laparoscopic and Open Surgical Resection of Clear Cell Renal Cell Carcinoma

Stephen P. Povoski, MD[1], Nathan C. Hall, MD, PhD[1], Douglas A. Murrey Jr, MD, MS[1], David S. Sharp, MD[1], Charles L. Hitchcock, MD, PhD[1], Cathy M. Mojzisik, RN, MS[1], Eamonn E. Bahnson, BA[1], Michael V. Knopp, MD, PhD[1], Edward W. Martin Jr, MD[1], and Robert R. Bahnson, MD[1]

Abstract

Renal cell carcinoma (RCC) accounts for approximately 85% to 90% of all primary kidney malignancies, with clear cell RCC (ccRCC) constituting approximately 70% to 85% of all RCCs. This study describes an innovative multimodal imaging and detection strategy that uses ^{124}I-labeled chimeric monoclonal antibody G250 (^{124}I-cG250) for accurate preoperative and intraoperative localization and confirmation of extent of disease for both laparoscopic and open surgical resection of ccRCC. Two cases presented herein highlight how this technology can potentially guide complete surgical resection and confirm complete removal of all diseased tissues. This innovative ^{124}I-cG250 (ie, ^{124}I-girentuximab) multimodal imaging and detection approach, which would be clinically very useful to urologic surgeons, urologic medical oncologists, nuclear medicine physicians, radiologists, and pathologists who are involved in the care of ccRCC patients, holds great potential for improving the diagnostic accuracy, operative planning and approach, verification of disease resection, and monitoring for evidence of disease recurrence in ccRCC patients.

Keywords

image-guided surgery, surgical oncology, urology

Introduction

Renal cell carcinoma (RCC), which arises from the renal tubular epithelial cells,[1-4] accounts for approximately 85% to 90% of all primary kidney malignancies.[5-7] Clear cell RCC (ccRCC) constitutes approximately 70% to 85% of all RCCs, followed by papillary RCC (8% to 15%), chromophobe RCC (2% to 5%), and a variety of other rare histologic subtypes.[8-14]

In 1986, the IgG monoclonal antibody (mAb) Grawitz 250 (G250) was first described in the literature by Oosterwijk et al[15,16] at the University of Leiden in The Netherlands. Of historical interest, the basis of the name Grawitz 250 is best explained by the developer of this mAb (Egbert Oosterwijk, personal communication, July 11 and October 26, 2011). Mice were immunized with kidney tumor homogenates, and all the hybridoma clones

[1]The Ohio State University Medical Center, Columbus, OH, USA

Corresponding Author:
Stephen P. Povoski, Department of Surgery, The Ohio State University Medical Center, N-924 Doan Hall, 410 West 10th Avenue, Columbus, OH 43210, USA
Email: stephen.povoski@osumc.edu

derived from the mice were named in consecutive series with the letter G, followed by a number. The letter G was selected by Oosterwijk to stand for Grawitz, in recognition of Paul Albert Grawitz (1850-1932), a German pathologist and professor at the University of Greifswald from 1886 to 1921, who is credited in the urologic literature with the first description of RCC in 1883 (ie, Grawitz's tumor).[17,18] The number 250 simply represented the fact that this particular hybridoma clone was the 250th hybridoma clone derived from mice immunized with kidney tumor homogenates, thus forming the basis of the derivation for the name Grawitz 250 (ie, G250). Even at its inception in 1986, Oosterwijk et al[15] clearly recognized the great potential of G250 for radioimmunoimaging.

Monoclonal antibody G250 recognizes the antigen carbonic anhydrase IX (CA IX).[16,19] CA IX antigen is a cytosolic transmembrane glycoprotein.[19-21] It represents one of many carbonic anhydrase enzymes that are involved in catalyzing the reaction $CO_2 + H_2O \leftrightarrow HCO_3^- + H^+$, a process ultimately important in the regulation of proton flux in cells and in pH regulation.[19,20] The catalytic site for CA IX is located extracellularly, where it is involved in creating an acidic microenvironment.[19,22] CA IX expression has been shown to be induced by hypoxia,[23,24] and it may have prognostic implications for evaluating disease progression and response to therapy.[21,25,26]

It is well established that CA IX antigen is constitutively expressed by 97% to 98% of all ccRCC,[15,16,19,21,25,27-29] in both primary and metastatic disease.[15,16,19,21,25,27-29] Yet it is absent from normal kidney tissues, including normal adult proximal tubular epithelial cells and fetal kidney tissue.[15,16,19,27-29] Likewise, it is more minimally expressed or absent in other, much less common renal epithelial neoplasms, including papillary RCC, chromophobe RCC, and oncocytoma.[21] A variety of other tumors (ie, carcinomas of the uterine cervix, esophagus, colon, lung, breast, brain, and vulva)[19,27] and normal adult human tissues (ie, gastric mucosa, small intestinal mucosal crypts, liver, and pancreatobiliary epithelium)[15,21,28,29] have been shown to have varying degrees of CA IX expression. However, this is generally to a much lesser degree than is seen in ccRCC and has greater heterogeneity. CA IX expression has not been demonstrated in normal heart, lung, prostate, brain, muscle, peripheral blood, or placenta.[29]

The use of mAb G250 for the targeting of CA IX in ccRCC, and the resultant potential application related to radioimmunoimaging and various radioimmunotherapies, has long been recognized by Oosterwijk and colleagues.[15,16,19,30] In 1993, Oosterwijk et al[31] first reported on a phase I trial of ^{131}I-labeled murine mAb G250 (mG250) administered intravenously to preoperative patients with a clinical diagnosis of RCC, demonstrating safety and tumor localization by radioimmunoscintigraphy using whole-body planar gamma camera imaging in all patients with RCC expressing CA IX.[31] However, the occurrence of human anti-mouse antibodies (HAMA) in all the patients studied was thought to be a potential stumbling block for the use of mG250 for serial radioimmunoimaging and multiple-treatment radioimmunotherapy. To minimize the occurrence of HAMA response, a chimerized version of mAb G250 (cG250) was developed with the same affinity and binding characteristics as mG250.[30,32] In 1997, Steffens et al[32] reported on a phase I trial of ^{131}I-cG250 administered intravenously to preoperative patients with a clinical diagnosis of primary RCC, demonstrating safety and tumor localization by radioimmunoscintigraphy using whole-body planar gamma camera imaging in all patients with RCC expressing CA IX.[32] However, subsequent similar trials using ^{131}I-cG250 to assess radioimmunoscintigraphy with whole-body planar gamma camera imaging in patients with metastatic RCC revealed more variability in the reported degree of successful disease localization, ranging from 30% to 100%,[33-37] despite the fact that all these publications were reported by the same group of authors. This greater variability in the reported success of disease localization in patients with metastatic RCC may have been more a reflection of the limitation of the variability in the gamma camera imaging technology used during different phases of their investigations rather than that of the mAb G250 itself.

With continued improvements in positron emission tomography/computed tomography (PET/CT) technology, and the great potential for the use of the positron emitter ^{124}I with this technology,[38,39] increased interest has developed in the application of ^{124}I-cG250 for radioguided imaging and detection of ccRCC.[40,41] In 2007, Divgi et al[40] first reported on a pilot, phase I trial using intravenously administered ^{124}I-cG250 to assess preoperative PET/CT localization of kidney tumors in patients scheduled for surgical resection.[40] They found that 15 out of 16 (94%) ccRCCs were identified with ^{124}I-cG250 on PET/CT, whereas all 9 non-ccRCCs were nonvisualized.[40] In this regard, a larger, multi-institutional phase III industry-sponsored clinical trial[42-44] using ^{124}I-cG250 (ie, ^{124}I-girentuximab), in which The Ohio State University Medical Center (OSUMC) participated, has been subsequently undertaken and patient accrual completed. The initial reported results from this multi-institutional phase III industry-sponsored clinical trial have shown superiority of ^{124}I-cG250 PET/CT imaging over that of diagnostic CT imaging in the diagnosis of ccRCC.[44]

Most recently, the use of handheld radiation detection probe technology for intraoperative detection and localization of ccRCC using ^{124}I-cG250 and specimen PET/CT imaging of resected surgical specimens has been described in the literature.[45-47] Along similar lines, a comprehensive methodology of multimodal imaging and

detection during ^{18}F-fluorodeoxyglucose (^{18}F-FDG)-directed surgery for patients with known or suspected ^{18}F-FDG-avid malignancies has been previously described.[48-51] However, to date, an analogous multimodal imaging and detection approach for ^{124}I-cG250-directed surgery is yet to be reported.

To this point, the current report describes an innovative multimodal imaging and detection methodology that uses ^{124}I-cG250 for accurate preoperative and intraoperative localization and confirmation of extent of disease in both laparoscopic and open surgical resection of ccRCC. The 2 cases presented herein highlight this technology. In one case, this innovative strategy during a laparoscopic approach to ccRCC was instrumental in the intraoperative identification of all diseased tissues (including a retroperitoneal lymph node metastasis), in guiding complete surgical resection, and in the confirmation of complete removal of all diseased tissues, thus allowing for successful laparoscopic resection of both the primary and the metastatic sites of disease, which otherwise would not have been technically feasible. In the other case, this innovative strategy during an open right partial nephrectomy was instrumental in guiding complete surgical resection, in the confirmation of complete removal of the tumor, and in the assessment of the kidney parenchyma surgical resection margin.

Case Reports

Both patients were enrolled at OSUMC in a multi-institutional phase III industry-sponsored clinical trial (Wilex AG, Munich, Germany) comparing ^{124}I-based PET/CT imaging versus diagnostic CT imaging for the detection of ccRCC in presurgical patients with renal masses using ^{124}I-cG250.[42-44] As with any industry-sponsored clinical trial conducted at OSUMC, the protocol was reviewed by the OSUMC Office of Responsible Research Practices and reviewed and approved by the Western Institutional Review Board (Olympia, WA). The radiolabeling of cG250 with ^{124}I was performed by IBA Molecular North American (Richmond, VA).

Case 1

A 60-year-old Caucasian male with a history of Ollier disease (a rare, nonhereditary, sporadic disorder characterized by multiple intraosseous benign cartilaginous tumors) presented with a right renal mass that was found at the time of a work-up for painless hematuria. CT scan of the abdomen showed a 10.3 cm × 7.6 cm × 6.7 cm mass in the superior pole of the right kidney, with infiltration into the posterior hilum of the upper renal pole (Figure 1). Retrograde cystoscopy was completely negative.

^{18}F-FDG PET/CT imaging was performed during concomitant work-up of a suspicious left femoral head/neck lesion related to the patient's Ollier disease. ^{18}F-FDG PET/CT imaging was performed 89 minutes following intravenous administration of 15.3 mCi of ^{18}F-FDG (Figure 2). The attenuation correction non-contrast-enhanced CT portion of the ^{18}F-FDG PET/CT imaging showed a large mass arising from the superior pole of the right kidney, with ^{18}F-FDG activity less than or equal to that of the normal ^{18}F-FDG accumulation pattern within the remainder of either kidney. Mild, increased ^{18}F-FDG activity was seen in the left femoral head and neck region. No obvious sites of metastatic disease were originally identified in the initial interpretation of the ^{18}F-FDG PET/CT imaging.

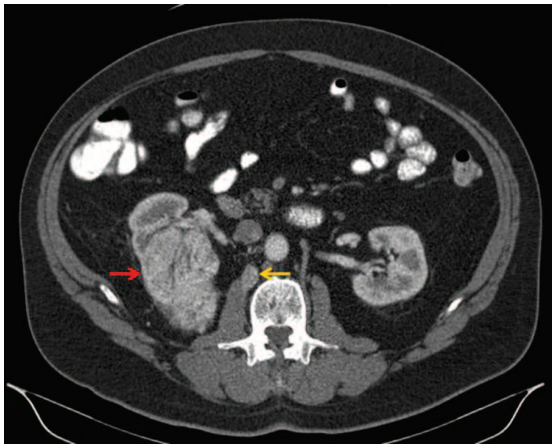

Figure 1. Diagnostic contrast-enhanced computed tomography (CT) of the abdomen (axial view) showing a solid mass in the superior pole of the right kidney (*red arrow*). This lesion demonstrated contrast enhancement with delayed washout having a density prior to intravenous contrast of 30 Hounsfield units (HU), 150 HU after contrast administration, and 58 HU in the excretion phase, suspicious for clear cell renal cell carcinoma. In retrospect, the small retroperitoneal lymph node (*yellow arrow*), which was not originally identified in the initial interpretation of the prior contrast-enhanced CT of the abdomen or the ^{18}F-fluorodeoxyglucose positron emission tomography (PET)/CT, was later first identified on ^{124}I-labeled chimeric monoclonal antibody G250 PET/CT and proven to represent a retroperitoneal lymph node metastasis by light microscopy.

^{124}I-cG250 PET/CT imaging was performed 4 days following intravenous administration of 5.4 mCi of ^{124}I-cG250 (Figure 3). ^{124}I-cG250 PET/CT imaging showed increased ^{124}I-cG250 activity within the renal mass in the superior pole of the right kidney, as well as increased ^{124}I-cG250 activity within a retroperitoneal lymph node.

The patient was taken to the operating room and underwent a laparoscopic right radical nephrectomy with retroperitoneal lymph node dissection. Intraoperatively, a laparoscopic gamma detection probe (Neoprobe Model 2059, Neoprobe Corporation, Dublin, OH) was used to

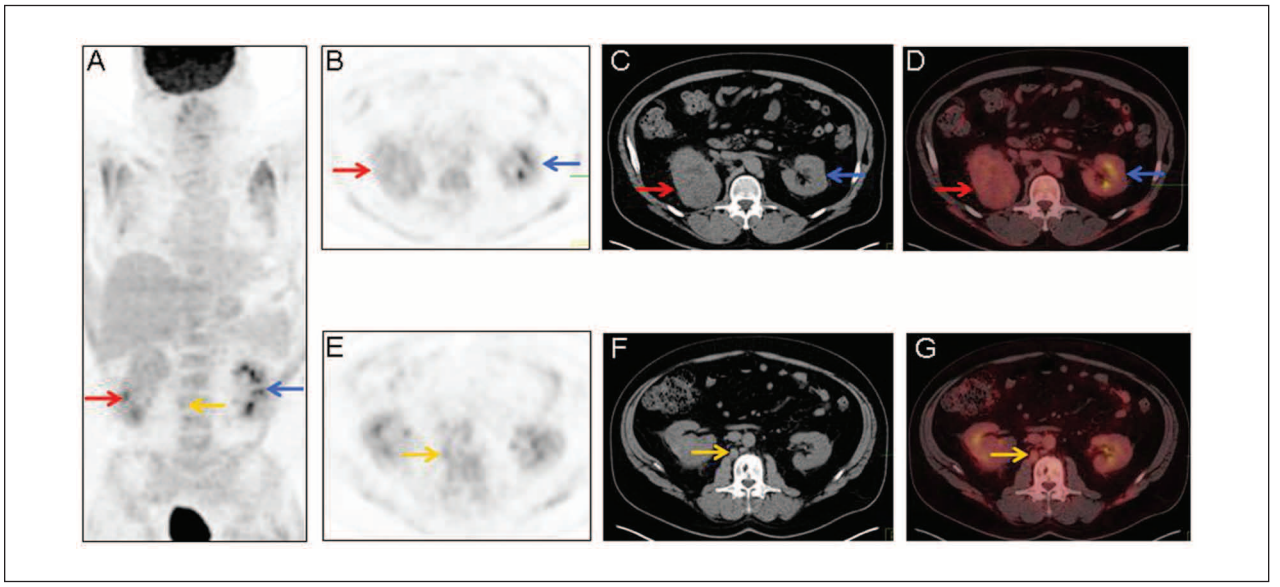

Figure 2. Maximum-intensity projection image (A), axial ^{18}F-fluorodeoxyglucose positron emission tomography (^{18}F-FDG PET) images (B and E), axial attenuation correction non-contrast-enhanced computed tomography (CT) images for ^{18}F-FDG PET localization (C and F), and fused axial ^{18}F-FDG PET/CT images (D and G) demonstrating physiologic renal ^{18}F-FDG activity (A, B, D, E, and G; *blue arrows*) and showing a mass on the attenuation correction non-contrast-enhanced CT (C; *red arrow*) that corresponds to the mass seen on the prior diagnostic contrast-enhanced CT of the abdomen in Figure 1. Note that the amount of ^{18}F-FDG activity within the mass (A, B, and D; *red arrows*) was less than or equal to that of the normal ^{18}F-FDG accumulation pattern within the remainder of either kidney. In retrospect, the small retroperitoneal lymph node (A, E, F, and G; *yellow arrows*), which was not originally identified in the initial interpretation of the prior diagnostic contrast-enhanced CT of the abdomen or the ^{18}F-FDG PET/CT, was later first identified on ^{124}I-labeled chimeric monoclonal antibody G250 PET/CT and proven to represent a retroperitoneal lymph node metastasis on light microscopy.

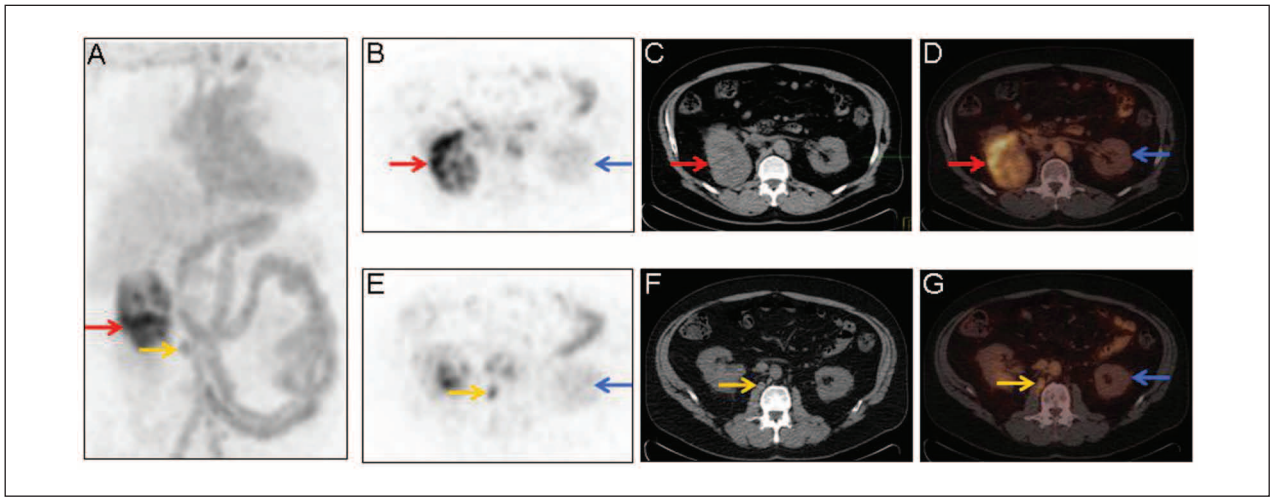

Figure 3. Maximum-intensity projection image (A), axial ^{124}I-labeled chimeric monoclonal antibody G250 (^{124}I-cG250) positron emission tomography (PET) images (B and E), axial attenuation correction non-contrast-enhanced computed tomography (CT) for ^{124}I-cG250 PET localization (C and F), and fused axial ^{124}I-cG250 PET/CT images (D and G) demonstrating significant ^{124}I-cG250 activity in the superior portion of the right kidney (A, B, and D; *red arrows*) that corresponds to the mass seen on the prior diagnostic contrast-enhanced CT of the abdomen in Figure 1. Note that there is little to no ^{124}I-cG250 accumulation in the normal kidney (B, D, E, and G; *blue arrows*). Additionally, on ^{124}I-cG250 PET/CT imaging, there is increased focal ^{124}I-cG250 activity within a small retroperitoneal lymph node (A, E, and G; *yellow arrows*), which was not originally identified in the initial interpretation of the prior diagnostic contrast-enhanced CT of the abdomen or the ^{18}F-fluorodeoxyglucose PET/CT. This small retroperitoneal lymph node (A, E, F, and G; *yellow arrows*) was later successfully identified and resected with the aid of a laparoscopic gamma detection probe at the time of laparoscopic right radical nephrectomy and retroperitoneal lymph node dissection.

localize and identify all sites of ^{124}I-cG250 uptake, to assist in the surgical resection, and for confirmation of complete removal of all sites of increased ^{124}I-cG250 activity. The laparoscopic gamma detection probe correctly identified increased ^{124}I-cG250 activity, both within the primary tumor of the right kidney and within the adjacent retroperitoneal lymph node tissues and provided confirmation of successful laparoscopic surgical resection.

The intact right radical nephrectomy specimen and the intact retroperitoneal lymph node dissection specimen were imaged with ^{124}I-cG250 PET/CT imaging and underwent subsequent standard pathology processing and microscopic evaluation (Figure 4). ^{124}I-cG250 PET/CT imaging clearly identified the sites of disease within the intact right radical nephrectomy specimen and the intact retroperitoneal lymph node dissection specimen. Histopathologic evaluation of the right nephrectomy specimen revealed an RCC (Fuhrman grade 3, 10.5 cm × 7.4 cm × 5.8 cm) of the clear cell type with sarcomatoid features. It had surgical resection margins that were negative, including Gerota's fascia, the renal vessels, and the distal ureter. A total of 5 regional lymph nodes were identified within the retroperitoneal lymph node dissection specimen, with one lymph node metastasis identified and representing a lymph node nearly completely replaced by a tumor that was initially recognized on the preoperative ^{124}I-cG250 PET/CT imaging and resected with the assistance of the laparoscopic gamma detection probe.

The patient had a relatively uneventful postoperative course and was discharged to home on postoperative day 1. Two weeks later, the patient subsequently underwent an uneventful left proximal femur hemiarthroplasty, which showed a low-grade cartilaginous neoplasm, consistent with his Ollier disease. The patient then went on to participate in the ASSURE (ECOG 2805) clinical trial, representing a randomized, double-blind, multi-institutional, phase III clinical trial comparing adjuvant sorafenib versus adjuvant sunitinib versus placebo in patients with resected RCC. At the time of this publication—30 months after the patient's previous laparoscopic right radical nephrectomy and retroperitoneal lymph node dissection—the patient is without evidence of disease.

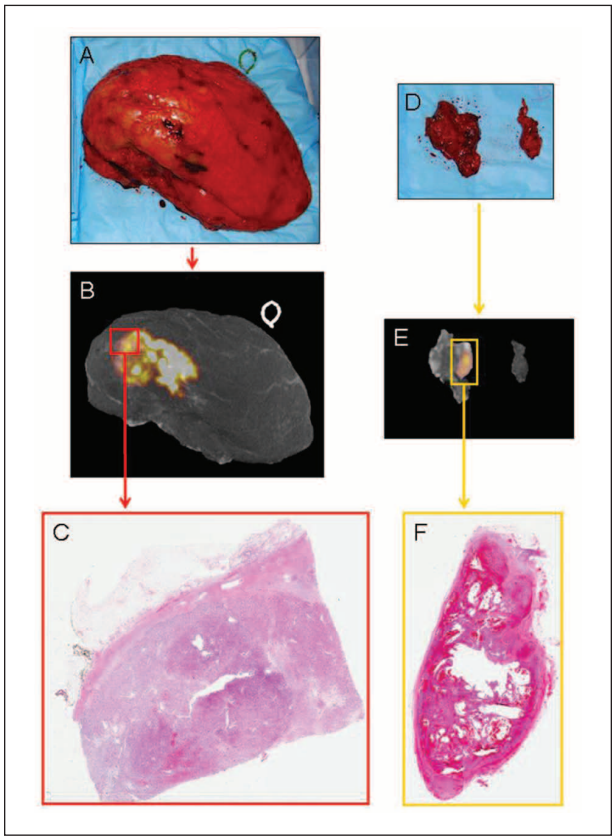

Figure 4. Digital photograph of the intact right radical nephrectomy specimen (A) with ^{124}I-labeled chimeric monoclonal antibody G250 (^{124}I-cG250) positron emission tomography (PET)/computed tomography (CT) three-dimensional (3D) reconstruction (B) demonstrating a heterogeneous area of increased ^{124}I-cG250 activity and corresponding to the histopathologically proven clear cell renal cell carcinoma primary tumor (C), as seen on light microscopy (hematoxylin and eosin [H&E]-stained, whole-mount slide, 0.4× magnification). Digital photograph of the intact retroperitoneal lymph node dissection specimen (D) with ^{124}I-cG250 PET/CT 3D reconstruction (E) demonstrating focal increased ^{124}I-cG250 activity and a corresponding single lymph node that was found to contain histopathologically proven metastatic clear cell renal cell carcinoma (F), as seen on light microscopy (H&E-stained, whole-mount slide, 0.3× magnification).

Case 2

A 39-year-old Caucasian female with a previous history of renal calculi presented for evaluation of right flank pain. Ultrasound of the abdomen showed a 1.9 cm × 1.6 cm × 1.4 cm solid-appearing lesion in the inferior pole of the right kidney. CT of the abdomen showed a 2.0 cm × 1.9 cm × 1.9 cm intraparenchymal mass within the posterior cortex of the inferior pole of the right kidney (Figure 5).

^{124}I-cG250 PET/CT imaging was performed 5 days following intravenous administration of 5.2 mCi of ^{124}I-cG250 (Figure 6). ^{124}I PET/CT imaging showed increased ^{124}I-cG250 activity within the renal mass in the inferior pole of the right kidney.

The patient was taken to the operating room and underwent an open right partial nephrectomy of the inferior pole of the right kidney. At the discretion of the

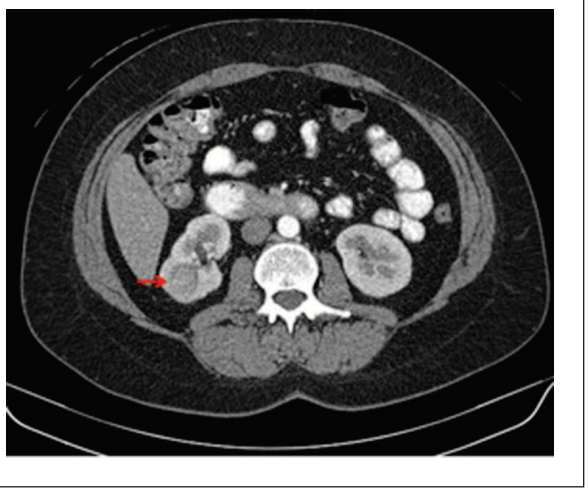

Figure 5. Diagnostic contrast-enhanced computed tomography (CT) of the abdomen (axial view) showing a solid mass in the inferior pole of the right kidney (*red arrow*). This lesion demonstrated contrast enhancement with delayed washout having a density prior to intravenous contrast of 39 Hounsfield units (HU), 111 HU after contrast administration, and 83 HU in the excretion phase, suspicious for clear cell renal cell carcinoma.

surgeon, an intraoperative gamma detection probe was not used in this case.

The intact and bisected right partial nephrectomy specimens were imaged with ^{124}I PET/CT imaging (Figure 7). ^{124}I-cG250 PET/CT imaging clearly identified the tumor size and location within the intact and bisected specimens and the relationship of the tumor to the parenchymal surgical resection margin surface within the bisected specimen.

The right partial nephrectomy specimen underwent subsequent standard pathology processing and microscopic evaluation (Figure 7). Histopathologic evaluation of the right partial nephrectomy specimen revealed an RCC (Fuhrman grade 2, 1.7 cm × 1.5 cm × 1.4 cm) of the clear cell type. It had negative surgical resection margins, with the closest distance measuring 0.7 cm from the inked parenchymal surgical resection margin surface of the right partial nephrectomy specimen, which correlated well with the ^{124}I-cG250 PET/CT image of the bisected right partial nephrectomy specimen.

The patient had a relatively uneventful postoperative course and was discharged to home on postoperative day 2. The patient required no postoperative adjuvant therapies. At the time of this publication—36 months after her previous open right partial nephrectomy—the patient is without evidence of disease.

Discussion

^{18}F-FDG PET/CT imaging is currently considered the standard of care for the molecular imaging of many solid malignancies.[52-57] However, ^{18}F-FDG PET/CT imaging has the inherent limitation of being non-cancer-specific, resulting in the accumulation of ^{18}F-FDG in many non-cancer-bearing tissues, including accumulation within tissues representing benign disease processes (ie, infection, inflammation, and trauma) and within normal tissues (ie, brain, heart, mucosa and smooth muscle of the stomach, small intestines and colon, thyroid, liver, spleen, kidneys, ureters, and bladder) that have a normal physiologic propensity to accumulate ^{18}F-FDG.[52-56,58-65] As a result of this inherent limitation of ^{18}F-FDG, the specificity and sensitivity of ^{18}F-FDG PET/CT for cancer imaging have been negatively affected. This is especially evident for certain cancer types (ie, RCC, bladder cancer, and prostate cancer) that typically are located in close proximity to anatomic structures with high physiologic ^{18}F-FDG activity (ie, kidneys, ureters, and bladder). This negative effect on the specificity and sensitivity of ^{18}F-FDG PET/CT for cancer imaging is truly a reflection of an intrinsic challenge of such imaging as it relates to the issue of background activity and is not necessarily a reflection of the available signal.[66] This intrinsic background activity dilemma remains the major limiting factor of ^{18}F-FDG PET/CT for cancer imaging.

In this specific regard, the background activity challenges can be significantly improved on for PET/CT imaging of cancer when one considers coupling a positron-emitting radionuclide, such as ^{124}I, with a molecular targeting agent that is cancer specific, such as cG250, which is nearly ubiquitously and constitutively expressed by all ccRCCs but has low to no expression in most normal adult human tissues. There are exceptions to this rule in normal adult human tissues, such as gastric mucosa, small intestinal mucosal crypts, liver, and pancreatobiliary epithelium, to which the molecular targeting agent cG250 can bind, but generally to more varying and less intense degrees than seen with ccRCC.[15,21,28,29] To his great credit, the potential of mAb G250 for targeting CA IX in ccRCC and for use in various radioimmunoimaging and radioimmunotherapy applications has long been recognized by Oosterwijk.[15,16,19,30]

The development of an innovative multimodal imaging and detection strategy that effectively uses ^{124}I-cG250 for the management of ccRCC would be clinically very useful to urologic surgeons, urologic medical oncologists, nuclear medicine physicians, radiologists, and pathologists who are involved in the care of ccRCC patients.[46] This innovative ^{124}I-cG250 multimodal imaging and

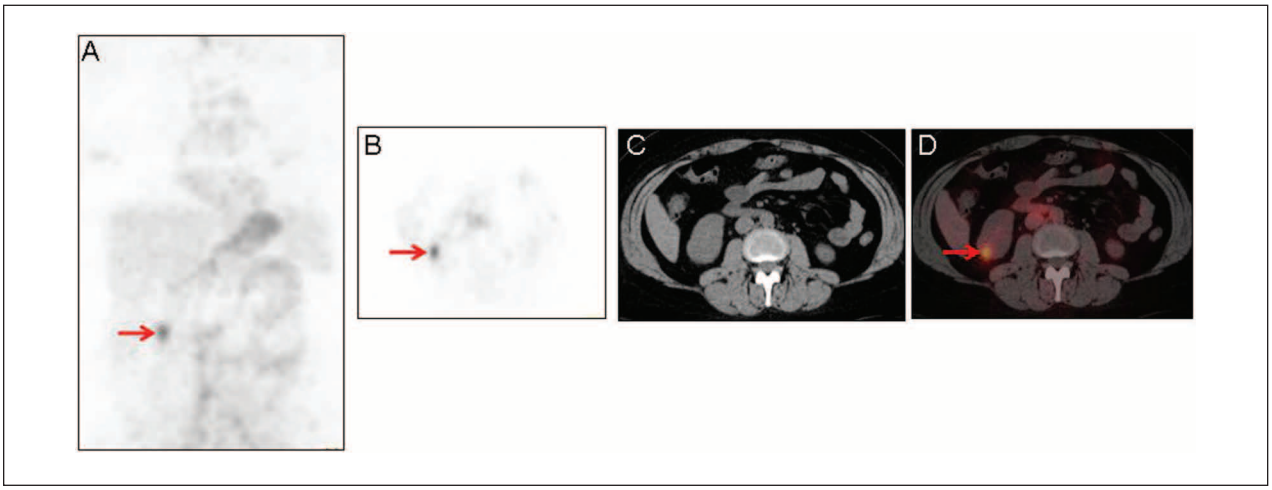

Figure 6. Maximum-intensity projection image (A), axial ^{124}I-labeled chimeric monoclonal antibody G250 (^{124}I-cG250) positron emission tomography (PET) image (B), axial attenuation correction non-contrast-enhanced computed tomography (CT) for ^{124}I-cG250 PET localization (C), and fused axial ^{124}I-cG250 PET/CT image (D) demonstrating increased ^{124}I-cG250 activity in the inferior pole of the right kidney (A, B, and D; *red arrows*) that corresponds to the mass seen on the prior diagnostic contrast-enhanced CT of the abdomen in Figure 5. Note that there is little to no ^{124}I-cG250 activity in the remainder of either kidney.

detection methodology could potentially be instrumental in (*a*) accurately localizing and identifying all sites of disease and the extent of disease, (*b*) assisting in the surgical resection and confirmation of complete removal of all sites of disease, and (*c*) monitoring patients for evidence of recurrence of disease after previous surgical resection. Such an innovative ^{124}I-cG250 multimodal imaging and detection strategy would be useful for accurate preoperative and intraoperative localization and confirmation of complete removal of all sites of disease during both laparoscopic and open surgical resection of ccRCC, as well as for cases with or without known/suspected regional lymph node involvement. In particular, as it pertains to laparoscopic surgical resection of patients with ccRCC, this ^{124}I-cG250 multimodal imaging and detection strategy may allow for identification and complete surgical resection of the known primary tumor and of any sites of occult disease (ie, regional lymph node metastases) by a minimally invasive laparoscopic surgical approach, which otherwise would not be technically feasible without a specific molecular targeting approach with ^{124}I-cG250. Likewise, as it pertains to attempted partial nephrectomy by either a laparoscopic or an open surgical resection approach for patients with early-stage ccRCC, this ^{124}I-cG250 multimodal imaging and detection strategy may improve the success rate of complete surgical resection by assisting the urologic surgeon and the pathologist in the assessment of the kidney parenchyma surgical resection margin. Last, as it pertains to radical nephrectomy by either a laparoscopic or an open surgical resection approach for patients with more advanced but still potentially surgically resectable carcinoma (ie, with larger primary tumors and/or bulky regional lymph node involvement), this ^{124}I-cG250 multimodal imaging and detection strategy may be of assistance to the urologic surgeon for intraoperative guidance on the exact extent of disease and for confirmation of complete surgical resection.

Conclusions

Herein, an innovative multimodal imaging and detection strategy that uses ^{124}I-cG250 for accurate preoperative and intraoperative localization and confirmation of extent of disease for ccRCC has been described. In one case, the use of this innovative strategy during a laparoscopic approach to ccRCC was instrumental in the intraoperative identification of all diseased tissues (including a retroperitoneal lymph node metastasis), in guiding complete surgical resection, and in the confirmation of complete removal of all diseased tissues, thus allowing for successful laparoscopic resection of both the primary and the metastatic sites of disease, which otherwise would not have been technically feasible. In the other case, this innovative strategy during an open right partial nephrectomy was instrumental in guiding complete surgical resection, in the confirmation of complete removal of the tumor, and in the assessment of the kidney paren-

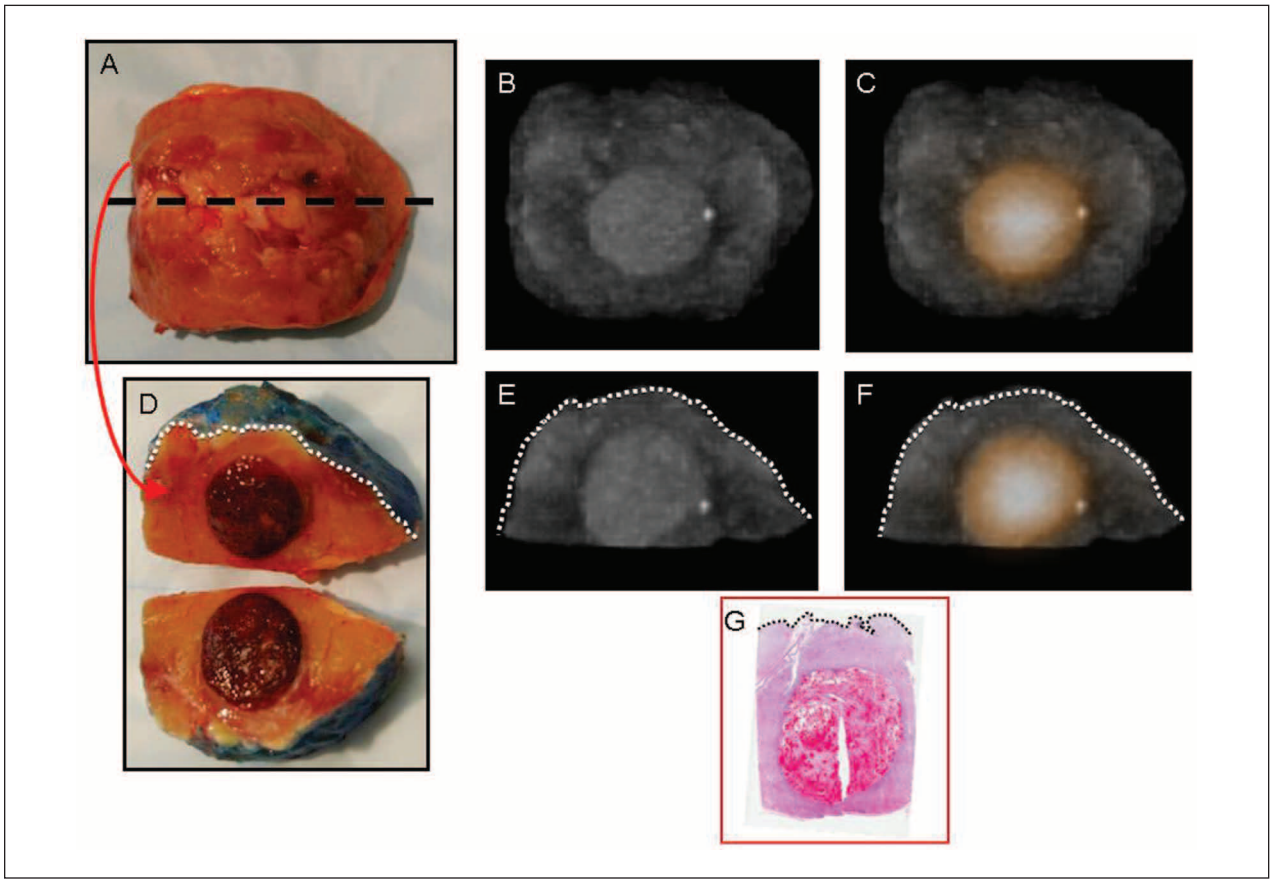

Figure 7. Digital photograph of the intact right partial nephrectomy specimen (A), with computed tomography (CT) three-dimensional (3D) reconstruction (B) demonstrating an ovoid hyperdensity in the center of the intact specimen and with ^{124}I-labeled chimeric monoclonal antibody G250 (^{124}I-cG250) positron emission tomography (PET)/CT 3D reconstruction (C) demonstrating an ovoid area of increased ^{124}I-cG250 activity in the center of the intact specimen. Digital photograph of the bisected right partial nephrectomy specimen, grossly demonstrating an ovoid tumor mass (D). The cut-surface edge of the parenchymal surgical resection margin of the right partial nephrectomy specimen was painted with blue ink prior to bisection. The black dashed line in panel A corresponds to the plane of bisection of the right partial nephrectomy specimen in panel D. CT 3D reconstruction of the bisected right partial nephrectomy specimen (E) demonstrates an ovoid hyperdensity in the center of the bisected specimen. The ^{124}I-cG250 PET/CT 3D reconstruction of the bisected right partial nephrectomy specimen (F) demonstrates an ovoid area of increased ^{124}I-cG250 activity, of a similar shape and distribution, in the center of the bisected specimen. The white dotted line in panels D, E, and F represents the cut-surface edge of the blue-inked parenchymal surgical resection margin of the bisected right partial nephrectomy specimen (D). Note that the CT 3D reconstruction image of the bisected specimen (E) and the ^{124}I-cG250 3D PET/CT reconstruction image of the bisected specimen (F) both demonstrate that the ovoid hyperdensity and area of intense ^{124}I-cG250 activity, respectively, do not extend to the parenchymal surgical resection margin surface. Digital microphotograph (G) of the 1.7 cm × 1.5 cm × 1.4 cm clear cell renal cell carcinoma with a negative parenchymal surgical resection margin, as seen on light microscopy (hematoxylin and eosin–stained, whole-mount slide, 0.3× magnification). The black dotted line in panel G represents the cut-surface edge of the parenchymal surgical resection margin of the bisected right partial nephrectomy specimen (D).

chyma surgical resection margin. This multimodal approach, which would be clinically very useful to urologic surgeons, urologic medical oncologists, nuclear medicine physicians, radiologists, and pathologists who are involved in the care of ccRCC patients, holds great potential for improving the diagnostic accuracy, operative planning and approach, verification of disease resection, and monitoring for evidence of disease recurrence in patients with ccRCC.

Acknowledgments

The authors are very grateful to Darlene M. Meeks of The Ohio State University Medical Center (OSUMC) Radiology 3D Lab for her assistance with CT 3D image reconstruction, used to portray selected images in Figure 4 and Figure 7; to William Bennett, Deborah Hurley, Wendy Wilt, Marlene Wagonrod, Nichole Storey, and Carley Hartings from the Department of Radiology at OSUMC; to George Hinkle, Sonny Edwards,

Rodd Reinhart, and Aaron Haynam from the OSUMC Nuclear Pharmacy; and to Debra Zynger and Lawrence De Renne from the Department of Pathology at OSUMC.

Authors' Note

The authors had full control of the design of this study, data analysis/interpretation, writing of this article, and decision to submit the article for publication.

Declaration of Conflicting Interests

As disclosure of financial support for the publication of this article, we acknowledge that this study was supported by funds from IBA Molecular North America, Inc. (Dulles, Virginia) and Wilex AG (Munich, Germany) for payment of the fee for publication of the color figures and for payment of the fee for SAGE Choice.

Funding

The authors disclosed receipt of the following financial support for the research, authorship, and/or publication of this article: This study was supported by funds from IBA Molecular North America, Inc. (Dulles, Virginia) and Wilex AG (Munich, Germany) for payment of the fees for publication of the color figures and for SAGE Choice.

References

1. Pilcher JT. Carcinoma of the kidney. *Ann Surg*. 1921;73:301-309.
2. Oberling C, Riviere M, Haguenau F. Ultrastructure of the clear cells in renal carcinomas and its importance for the demonstration of their renal origin. *Nature*. 1960;186:402-403.
3. Braunstein H, Adelman JU. Histochemical study of the enzymatic activity of human neoplasms. II. Histogenesis of renal cell carcinoma. *Cancer*. 1966;19:935-938.
4. Wallace AC, Nairn RC. Renal tubular antigens in kidney tumors. *Cancer*. 1972;29:977-981.
5. Eble JN, Togashi K, Pisani P. Renal cell carcinoma. In Eble JN, Sauter G, Epstein JI, Sesterhenn IA, ed. *World Health Organization Classification of Tumours: Pathology and Genetics of Tumours of the Urinary System and Male Genital Organs*. Lyon, France: IARC Press; 2004:10-12.
6. National Cancer Institute, Division of Cancer Control and Population Science, Surveillance Research Program, Cancer Statistics Branch. SEER Program Public Use Data Tapes 1973-2002. April 2005.
7. Lipworth L, Tarone RE, McLaughlin JK. The epidemiology of renal cell carcinoma. *J Urol*. 2006;176(6 pt 1): 2353-2358.
8. Kovacs G, Akhtar M, Beckwith BJ, et al. The Heidelberg classification of renal cell tumours. *J Pathol*. 1997;183:131-133.
9. Amin MB, Amin MB, Tamboli P, et al. Prognostic impact of histologic subtyping of adult renal epithelial neoplasms: an experience of 405 cases. *Am J Surg Pathol*. 2002;26:281-291.
10. Renshaw AA. Subclassification of renal cell neoplasms: an update for the practising pathologist. *Histopathology*. 2002;41:283-300.
11. Cheville JC, Lohse CM, Zincke H, Weaver AL, Blute ML. Comparisons of outcome and prognostic features among histologic subtypes of renal cell carcinoma. *Am J Surg Pathol*. 2003;27:612-624.
12. Gudbjartsson T, Hardarson S, Petursdottir V, Thoroddsen A, Magnusson J, Einarsson GV. Histological subtyping and nuclear grading of renal cell carcinoma and their implications for survival: a retrospective nation-wide study of 629 patients. *Eur Urol*. 2005;48:593-600.
13. Prasad SR, Humphrey PA, Catena JR, et al. Common and uncommon histologic subtypes of renal cell carcinoma: imaging spectrum with pathologic correlation. *Radiographics*. 2006;26:1795-1806; discussion 1806-1810.
14. Aydin H, Zhou M. The changing face of renal cell carcinoma pathology. *Curr Oncol Rep*. 2008;10:235-244.
15. Oosterwijk E, Ruiter DJ, Hoedemaeker PJ, et al. Monoclonal antibody G 250 recognizes a determinant present in renal-cell carcinoma and absent from normal kidney. *Int J Cancer*. 1986;38:489-494.
16. Oosterwijk E. Carbonic anhydrase IX: historical and future perspectives. *BJU Int*. 2008;101(suppl 4):2-7.
17. Grawitz P. Die sogenannten Lipome der Niere. *Virchows Archiv für pathologische Anatomie und Physiologie, und für klinische Medicin*. 1883;93:39-63.
18. Mccormick WF, Blake CC. Some notes on Paul Grawitz and his tumor. *Cancer*. 1958;11:871-872.
19. Stillebroer AB, Mulders PF, Boerman OC, Oyen WJ, Oosterwijk E. Carbonic anhydrase IX in renal cell carcinoma: implications for prognosis, diagnosis, and therapy. *Eur Urol*. 2010;58:75-83.
20. Opavský R, Pastoreková S, Zelník V, et al. Human MN/CA9 gene, a novel member of the carbonic anhydrase family: structure and exon to protein domain relationships. *Genomics*. 1996;33:480-487.
21. Leibovich BC, Sheinin Y, Lohse CM, et al. Carbonic anhydrase IX is not an independent predictor of outcome for patients with clear cell renal cell carcinoma. *J Clin Oncol*. 2007;25:4757-4764.
22. Supuran CT. Carbonic anhydrases: catalytic and inhibition mechanisms, distribution and physiological roles. In: Supuran CT, Scozzafava A, Conway J, eds. *Carbonic Anhydrase: Its Inhibitors and Activators*. Boca Raton, FL: CRC Press; 2004:1-23.
23. Wykoff CC, Beasley NJ, Watson PH, et al. Hypoxia-inducible expression of tumor-associated carbonic anhydrases. *Cancer Res*. 2000;60:7075-7083.
24. Rice SL, Roney CA, Daumar P, Lewis JS. The next generation of positron emission tomography radiopharmaceuticals in oncology. *Semin Nucl Med*. 2011;41: 265-282.
25. Bui MH, Seligson D, Han KR, et al. Carbonic anhydrase IX is an independent predictor of survival in advanced renal clear cell carcinoma: implications for prognosis and therapy. *Clin Cancer Res*. 2003;9:802-811.

26. Phuoc NB, Ehara H, Gotoh T, et al. Prognostic value of the co-expression of carbonic anhydrase IX and vascular endothelial growth factor in patients with clear cell renal cell carcinoma. *Oncol Rep*. 2008;20: 525-530.
27. Liao SY, Aurelio ON, Jan K, Zavada J, Stanbridge EJ. Identification of the MN/CA9 protein as a reliable diagnostic biomarker of clear cell carcinoma of the kidney. *Cancer Res*. 1997;57:2827-2831.
28. Grabmaier K, Vissers JL, De Weijert MC, et al. Molecular cloning and immunogenicity of renal cell carcinoma-associated antigen G250. *Int J Cancer*. 2000;85:865-870.
29. Bismar TA, Bianco FJ, Zhang H, et al. Quantification of G250 mRNA expression in renal epithelial neoplasms by real-time reverse transcription-PCR of dissected tissue from paraffin sections. *Pathology*. 2003;35:513-517.
30. Oosterwijk E, Debruyne FM. Radiolabeled monoclonal antibody G250 in renal-cell carcinoma. *World J Urol*. 1995;13:186-190.
31. Oosterwijk E, Bander NH, Divgi CR, et al. Antibody localization in human renal cell carcinoma: a phase I study of monoclonal antibody G250. *J Clin Oncol*. 1993;11:738-750.
32. Steffens MG, Boerman OC, Oosterwijk-Wakka JC, et al. Targeting of renal cell carcinoma with iodine-131-labeled chimeric monoclonal antibody G250. *J Clin Oncol*. 1997;15:1529-1537.
33. Steffens MG, Boerman OC, de Mulder PH, et al. Phase I radioimmunotherapy of metastatic renal cell carcinoma with ^{131}I-labeled chimeric monoclonal antibody G250. *Clin Cancer Res*. 1999;5(10 suppl):3268s-3274s.
34. Brouwers AH, Dorr U, Lang O, et al. ^{131}I-cG250 monoclonal antibody immunoscintigraphy versus [18 F]FDG-PET imaging in patients with metastatic renal cell carcinoma: a comparative study. *Nucl Med Commun*. 2002;23:229-236.
35. Brouwers AH, Buijs WC, Oosterwijk E, et al. Targeting of metastatic renal cell carcinoma with the chimeric monoclonal antibody G250 labeled with (131)I or (111)In: an intrapatient comparison. *Clin Cancer Res*. 2003;9(10 pt 2):3953S-3960S.
36. Brouwers AH, Mulders PF, de Mulder PH, et al. Lack of efficacy of two consecutive treatments of radioimmunotherapy with ^{131}I-cG250 in patients with metastasized clear cell renal cell carcinoma. *J Clin Oncol*. 2005;23:6540-6548.
37. Brouwers AH, Mulders PF, Oyen WJ. Carbonic anhydrase IX expression in clear cell renal cell carcinoma and normal tissues: experiences from (radio) immunotherapy. *J Clin Oncol*. 2008;26:3808-3809; author reply 3811-3812.
38. Pentlow KS, Graham MC, Lambrecht RM, et al. Quantitative imaging of iodine-124 with PET. *J Nucl Med*. 1996;37:1557-1562.
39. Herzog H, Tellman L, Qaim SM, Spellerberg S, Schmid A, Coenen HH. PET quantitation and imaging of the non-pure positron-emitting iodine isotope 124I. *Appl Radiat Isot*. 2002;56:673-679.
40. Divgi CR, Pandit-Taskar N, Jungbluth AA, et al. Preoperative characterisation of clear-cell renal carcinoma using iodine-124-labelled antibody chimeric G250 (124I-cG250) and PET in patients with renal masses: a phase I trial. *Lancet Oncol*. 2007;8:304-310.
41. Leung K. ^{124}I-chimeric monoclonal antibody G250. http://www.ncbi.nlm.nih.gov/books/NBK43528/. Last updated May 20, 2010. Accessed October 5, 2011.
42. A comparative study of PET/CT versus diagnostic ct for the detection of clear cell renal cell carcinoma in pre-surgical patients with renal masses using iodine-124 labeled chimeric G250 (124I-cG250). http://clinicaltrials.gov/ct2/show/NCT00606632. Accessed October 5, 2011.
43. IBA/Wilex. Redectane: pre-BLA meeting with FDA, 17 June 2011. http://www.wilex.de/pdf/Download/20110617_WILEX_REDECTANE_PreBLA_Press_Analyst_presentation.pdf. Accessed October 5, 2011.
44. Uzzo R, Russo P, Chen D, et al. Multicenter phase 3 REDECT trial with iodine I 124 Girentuximab-PET/CT for the presurgical detection of clear cell renal cell carcinoma (ccRCC) [abstract]. *Kidney Cancer J*. 2010;8:79, 85.
45. Strong VE, Humm J, Russo P, et al. A novel method to localize antibody-targeted cancer deposits intraoperatively using handheld PET beta and gamma probes. *Surg Endosc*. 2008;22:386-391.
46. Bahnson EE, Murrey DA, Mojzisik CM, et al. PET/CT imaging of clear cell renal cell carcinoma with ^{124}I labeled chimeric antibody. *Ther Adv Urol*. 2009;1:67-70.
47. Murrey DA, Bahnson EE, Mojzisik CM, et al. Validation of targeted molecular imaging using surgical specimens: a feasibility assessment using 124I-cG250 monoclonal antibody PET/CT in clear cell renal cell carcinoma. *J Am Coll Surg*. 2009;209:s128.
48. Hall NC, Povoski SP, Murrey DA, Knopp MV, Martin EW. Combined approach of perioperative ^{18}F-FDG PET/CT imaging and intraoperative ^{18}F-FDG handheld gamma probe detection for tumor localization and verification of complete tumor resection in breast cancer. *World J Surg Oncol*. 2007;5:143.
49. Povoski SP, Hall NC, Walker MJ, Martin EW. Multimodality approach of perioperative ^{18}F-FDG PET/CT imaging, intraoperative ^{18}F-FDG handheld gamma probe detection, and intraoperative ultrasound for tumor localization and verification of resection of all sites of hypermetabolic activity in a case of occult recurrent metastatic melanoma. *World J Surg Oncol*. 2008;6:1.
50. Hall NC, Povoski SP, Murrey DA Jr, Knopp MV, Martin EW Jr. Bringing advanced medical imaging into the operative arena could revolutionize the surgical care of cancer patients. *Expert Rev Med Devices*. 2008;5:663-667.
51. Povoski SP, Hall NC, Murrey DA Jr, et al. Multimodal imaging and detection approach to ^{18}F-FDG-directed surgery for patients with known or suspected malignancies:

A comprehensive description of the specific methodology utilized in a single-institution cumulative retrospective experience. *World J Surg Oncol*. 2011;9:152.
52. Otsuka H, Graham M, Kubo A, Nishitani H. Clinical utility of FDG PET. *J Med Invest*. 2004;51:14-19.
53. Endo K, Oriuchi N, Higuchi T, et al. PET and PET/CT using 18F-FDG in the diagnosis and management of cancer patients. *Int J Clin Oncol*. 2006;11:286-296.
54. Maldonado A, González-Alenda FJ, Alonso M, Sierra JM. PET-CT in clinical oncology. *Clin Transl Oncol*. 2007;9: 494-505.
55. Otsuka H, Morita N, Yamashita K, Nishitani H. FDG-PET/CT for cancer management. *J Med Invest*. 2007;54:195-199.
56. Vallabhajosula S. (18)F-labeled positron emission tomographic radiopharmaceuticals in oncology: an overview of radiochemistry and mechanisms of tumor localization. *Semin Nucl Med*. 2007;37:400-419.
57. Poeppel TD, Krause BJ, Heusner TA, Boy C, Bockisch A, Antoch G. PET/CT for the staging and follow-up of patients with malignancies. *Eur J Radiol*. 2009;70:382-392.
58. Pauwels EK, Ribeiro MJ, Stoot JH, McCready VR, Bourguignon M, Mazière B. FDG accumulation and tumor biology. *Nucl Med Biol*. 1998;25:317-322.
59. Shields AF, Grierson JR, Dohmen BM, et al. Imaging proliferation in vivo with [F-18]FLT and positron emission tomography. *Nat Med*. 1998;4:1334-1336.
60. Lind P, Igerc I, Beyer T, Reinprecht P, Hausegger K. Advantages and limitations of FDG PET in the follow-up of breast cancer. *Eur J Nucl Med Mol Imaging*. 2004;31(suppl 1): S125-S134.
61. Lim HS, Yoon W, Chung TW, et al. FDG PET/CT for the detection and evaluation of breast diseases: usefulness and limitations. *Radiographics*. 2007;27(suppl 1): S197-S213.
62. Metser U, Even-Sapir E. Increased (18)F-fluorodeoxyglucose uptake in benign, nonphysiologic lesions found on whole-body positron emission tomography/computed tomography (PET/CT): accumulated data from four years of experience with PET/CT. *Semin Nucl Med*. 2007;37:206-222.
63. Sun D, Bloomston M, Hinkle G, et al. Radioimmunoguided surgery (RIGS), PET/CT image-guided surgery, and fluorescence image-guided surgery: past, present, and future. *J Surg Oncol*. 2007;96:297-308.
64. Schöder H, Moskowitz C. PET imaging for response assessment in lymphoma: potential and limitations. *Radiol Clin North Am*. 2008;46:225-241.
65. Povoski SP, Neff RL, Mojzisik CM, et al. A comprehensive overview of radioguided surgery using gamma detection probe technology. *World J Surg Oncol*. 2009; 7:11.
66. Frangioni JV. The problem is background, not signal. *Mol Imaging*. 2009;8:303-304.